Plasmons in layered nanospheres and nanotubes investigated by spatially resolved electron energy-loss spectroscopy

M. Kociak*
Laboratoire de Physique des Solides, Bâtiment 510, Université Paris-Sud, 91405 Orsay Cedex, France

L. Henrard
Laboratoire de Physique du Solide, Facultés Universitaires Notre-Dame de la Paix, 61 rue de Bruxelles, 5000 Namur, Belgium

O. Stéphan
Laboratoire de Physique des Solides, Bâtiment 510, Université Paris-Sud, 91405 Orsay Cedex, France

K. Suenaga
Laboratoire de Physique des Solides, Bâtiment 510, Université Paris-Sud, 91405 Orsay Cedex, France and JST-ICORP, Department of Physics, Meijo University, Nagoya 468-8502, Japan

C. Colliex
Laboratoire de Physique des Solides, Bâtiment 510, Université Paris-Sud, 91405 Orsay Cedex, France and Laboratoire Aimé Cotton, Bâtiment 505, Université Paris-Sud, 91405 Orsay Cedex, France
(Received 24 November 1999)

We present an extensive electron energy loss spectroscopy study of the low-loss energy region, recorded on multishell carbon and boron-nitride nanotubes and carbon hyperfullerenes. Collections of spectra were recorded in a scanning transmission electron microscope by scanning a subnanometer probe from vacuum into the center of the nano-objects. This experimental technique provides the unique ability of disentangling and identifying the different excitation modes of a nanoparticle. We concentrate on the study of surface modes excited in a near-field geometry where the coupling distance between the electron beam and the surface of the nano-objects is accurately monitored. Similarities between surface collective excitations in the different layered nanostructures (cylindrical or spherical, boron nitride, or carbon constituted) are pointed out. Two surface modes at 12–13 eV and 17–18 eV are experimentally clearly evidenced. We show that these modes are accurately described by a classical continuum dielectric model taking fully into account the anisotropic character and the hollow geometry of the nanoparticles. These two modes are shown to be directly related to the in-plane and out-of-plane components of the dielectric tensor. The higher-energy mode (in-plane mode) is shown to shift to higher energy with decreasing impact parameter, as a result of an increase in the weights of the high-order multipolar modes while reaching the surface of the nano-objects.

I. INTRODUCTION

The initial discovery of C_{60} by Kroto *et al.*[1] arose from studies on interstellar dust formation, and since then a large variety of new carbon closed shell structures have been synthesized leading to a revolution in the physical chemistry of carbon. Amongst these, let us mention onions and nanotubes made of carbon,[2,3] boron nitride,[4,5] or a mixture of B, C, and N.[6–8] From a structural point of view, all of these nanostructures can be described as the counterparts of layered planar materials within a spherical or cylindrical geometry. These new nanostructures were predicted to exhibit exciting properties. For example, while theoretical studies suggested that the band gap of carbon nanotubes should depend on their helicity and diameter,[9] boron nitride (BN) nanotubes were expected to have a constant band gap, independently of their helicity or diameter.[10] Such predictions were confirmed directly by transport spectroscopy measurements,[11] and the consequences for transport properties were pointed out.[12] More detailed descriptions of the properties of carbon onions[13,14] and nanotubes[14,15] can be found in recent reviews. On the other hand, the collective excitations in nanostructures have increasingly attracted the attention of the scientific community with the recent improved availability of prepared controlled nanoparticles or arrays of nanoparticles. For example, photonic devices such as photonic band-gap structures are now extensively studied and arrays of cylindrical holes have been shown to exhibit an extraordinary optical transmission due to coupled plasmon excitations.[16,17] Plasmon excitations are also related to the van der Waals interactions[18] that govern small particle self-organization and are also supposed to play a major role in new spectroscopic methods such as surface enhanced raman spectroscopy (SERS).[19] The present paper deals with the study of collective excitations (plasmons) in layered nanoparticles by electron energy loss spectroscopy (EELS) and their interpretation relying on simulation based on a semiclassical dielectric theory.

EELS is a powerful tool for the study of both the electronic structure and the dielectric properties of nano-objects. Low-loss energy spectra (in the 0–50 eV range) from small particles have been recorded by many authors studying sur-

face plasmons.[20–23] As far as plasmon excitations of carbon nanostructures are concerned, bulk π and $\pi+\sigma$ plasmons in C and BN nanotubes and C onions have been reported in several studies in transmission mode[24–28] and reflection mode,[29] but no global interpretation has been proposed to reconcile the different results. A surface plasmon mode was detected in C onions in reflection EELS (Ref. 29) and in carbon nanotubes in transmission EELS.[27]

The description of plasmon excitations as a solution of Maxwell's equations has been known since the pioneering work of Mie[30] and is the subject of many textbooks (see, for example, Ref. 31). The limit of validity of this theory for small atomic clusters has been studied more recently[32,33] giving rise to the conclusion that large nanoparticles, such as the ones studied in the present paper, can be described using dielectric bulk properties. Anisotropic layered structures have also been studied within the framework of Maxwell's equations.[34] However, the specificity of the spherical and cylindrical locally anisotropic particles under consideration here is to require an adapted extension of macroscopic theories. The peculiarity of the curved layered nano-objects is the coupling between the in-plane and the out-of-plane excitations, since the relative orientation of an external electromagnetic field (generated by an incident light or a charged particle) with the principal axis of the layers, is no longer defined over the entire particle. Recently, a dielectric model has been developed for this case and used to propose solutions to the initial interstellar dust puzzle[35] and to simulate EEL spectra.[36] Other approaches (i.e., hydrodynamic model,[37] multilayer two-dimensional electron gas approach,[38] and discrete dipoles approximation[39]) have also been developed, but a complete EELS simulation has only been realized within the dielectric theory[36] and, for small clusters, within the discrete dipoles approximation.[40]

In this paper, we present a detailed study of the low-loss energy region acquired across multishell carbon and BN onions and nanotubes in the context of a scanning transmission electron microscope (STEM). Collections of spectra were recorded while scanning a subnanometer probe under computer control (spectrum-image or spectrum-line modes[41]) from outside of the particle into the center of the particle. This mode allows a study of the excitation probability for the different modes as function of the impact parameter defined with an accuracy of 1 or 2 Å. In particular, the contribution of surface modes observed for a nonpenetrating beam can be disentangled from the whole EELS spectrum. In such nonpenetrating configurations, we probe the near-field decaying from the particle out into vacuum, with a fine control of the coupling distance between the electron beam and the surface of the nano-object. We find a very clear similarity between the excitations observed in spherical onions and in cylindrical nanotubes. We also underline the intensity and position variation of the EELS resonances with respect to the impact parameter. We interpret these valence excitations as collective surface modes within the framework of a classical continuum dielectric model, taking fully into account the anisotropic character and the hollow geometry of the objects.

II. EXPERIMENT

A. Samples description

In order to investigate the size and geometry effects on EEL spectra, we have analyzed a large collection of nanotubes and onions. The nanotubes were made of carbon and boron nitride. Carbon multiwall nanotubes (CMWNT) exhibited typical by 20–30 nm and 2–10-nm outer and inner radii, which corresponds to more than 15 layers. The boron nitride multiwall nanotubes (BNMWNT) were made of a much smaller number of layers, typically 4 or 5 layers. The carbon onions have a narrow range of diameters, namely, 15 nm and a vanishing inner cavity.

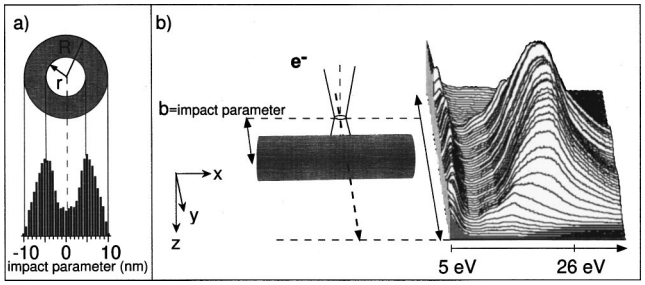

FIG. 1. (a) Definition of outer and inner radii (R and r, respectively) for a nanoparticle. High angle annular dark field (HADF) is shown as the way to accurately determine them. (b) Line spectrum across a multishell carbon nanotube of 20 nm outer diameter with corresponding scattering geometry.

B. Samples production

The CMWNT's were produced by a conventional arc-discharge method.[3] The formation of carbon onions on silver substrates has been achieved using an ion-implantation technique.[42] The silver substrate was then thinned from the free surface until a hole was drilled. BN nanotubes were synthesized by arc-discharge between HfB_2 electrodes in a nitrogen atmosphere.[5]

After ultrasonic dispersion in an ethanol solution, the nanotube containing powder is deposited on a holey carbon film for observation and spectroscopic measurements in a scanning transmission electron microscope.

C. Experiment

Measurements were performed on a STEM VG HB501 field emission gun operating at 100 keV and fitted with a Gatan 666 parallel-EELS spectrometer and a couple of high-angle annular detectors for simultaneous dark field mode imaging. Collections of spectra were acquired by scanning the 0.5–1-nm probe across a chosen isolated nano-object whose morphology (schematically described by an inner radius r and an outer radius R), was first identified by means of intensity profiles calculated from annular dark field (ADF) images [see Fig. 1(a)]. The beam was scanned from vacuum at large impact parameters into the object with spatial increments of 2.5 or 6 Å [Fig. 1(b)]. In order to obtain a high accuracy in the definition of the successive impact parameters, the annular dark field profile was simultaneously acquired. An unambiguous identification of the specific spectrum, in the line scan, corresponding to grazing incidence, is then possible. Each individual spectrum was recorded with a 0.4-s acquisition time and a 0.7-eV energy resolution. The objective and collection apertures were, respectively, 50 μm and 2 mm corresponding to a 7.5-mrad convergence angle and a 16.5-mrad collection angle, respectively. A typical se-

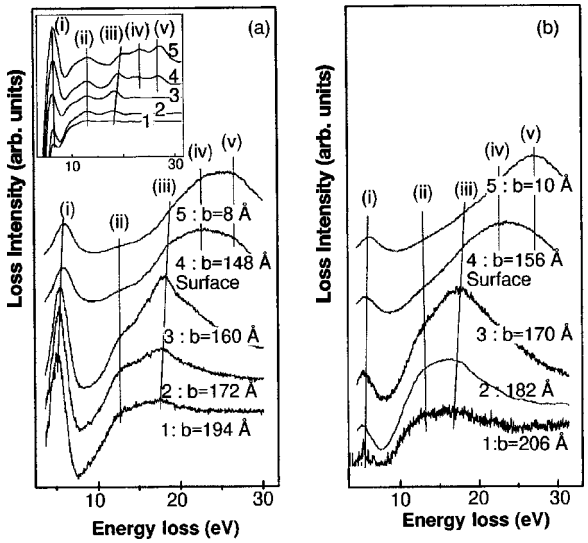

FIG. 2. Selections of spectra from line scans across a carbon multishell carbon nanotube (CMWNT) in (a) and a carbon onion in (b). Both nano-objects have similar external radii (150–200 Å). The values of the impact parameters are mentioned. In inset are shown the corresponding spectra in the second derivative mode for the same CMWNT. The different modes are labeled from (i) to (v).

quence of spectra acquired by scanning the probe perpendicular to the axis of a 26-shell carbon nanotube with external and internal radii of 20 nm and 11 nm, respectively, is displayed in Fig. 2(a). For an easier identification the same spectra are shown in the second derivative mode on the inset of Fig. 2(a). A similar line scan across an onion with a radius of 15 nm is displayed in Fig. 2(b). Figure 3 shows the intensity profiles for the different energy features in the carbon nanotube case together with the annular dark field profile. They were calculated by selecting a narrow energy window centered on each mode position. An intensity profile then results in the number of counts integrated over a given energy window (of a few eV) as a function of the probe position. From such an analysis, it is then possible to have access to the spatial dependence of the excitation probability of the

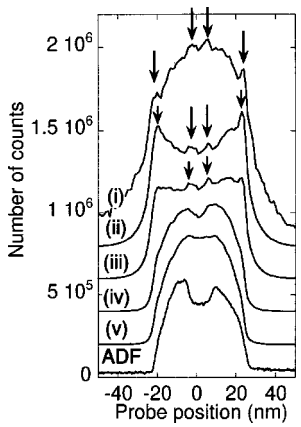

FIG. 3. Intensity profiles associated with the different modes seen in Fig. 2, when the beam is scanned across the carbon MWNT, shown together with the HADF profile. The profiles of surface modes (ii) and (iii) have four maxima located at the inner and outer surfaces of the nanotube. The profile of peak (i) shows both behaviors of surface and volume excitation.

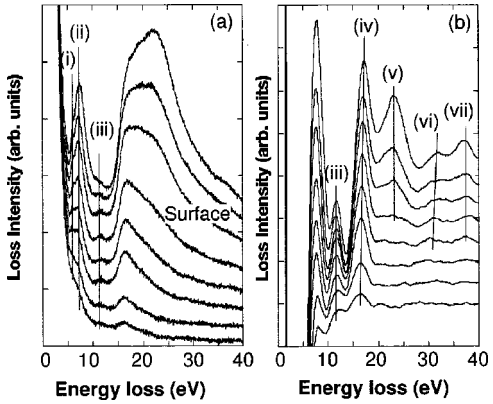

FIG. 4. Valence EEL spectra in the normal mode (a) and in the second derivative mode (b) extracted from a line scan across a BNMWNT that consists of 3–4 layers.

modes and then to classify modes into bulk and surface (evanescent) excitations by analyzing the decay into vacuum. Finally, results from a BN multishell nanotube with a 4-nm external radius are displayed in Fig. 4 in both normal and second derivative modes.

First, a general behavior of the evolution of the EEL spectrum can be identified for the whole set of analyzed nano-objects (C onions, BN, and C MWNT) as the electron beam is scanned across them. Three main energy features are detected for nonpenetrating geometries while three extra features (or four in case of BN) occur when the beam intersects the nano-objects. Later we will claim their common physical origin. Beyond this general behavior, the strong similarity between both results from carbon onions and carbon nanotubes in terms of mode energies has to be stressed. We will come back in Sec. III Å to the interpretation of this similarity between valence electronic excitations in graphitic particles of spherical and cylindrical geometries, respectively.

Let us start with the features occurring only for a penetrating beam into the solid. The corresponding pixels are correlated with a nonzero intensity in the ADF profile. As seen in Fig. 2, three main modes are detected around 6 eV (i), 23 eV (iv), and 27 eV (v) for carbon nano-objects (onions and MWNT). In the case of BN nanotubes (see Fig. 4), four main modes are detected at 7 eV (ii), 23 eV (v), 30 eV (vi), and 38 eV (vii).

For a nonpenetrating beam geometry, and when dealing with carbon nanotubes and carbon onions, three main energy peaks are observed at 6 eV (i), 13 eV (ii), and 17 eV (iii) at large impact parameters (more than 10 nm). The mode at 17 eV is shifting about 1 eV to higher energies when the beam-surface coupling distance is decreasing. Three main features are detected for small (3–4 walls) BNMWNT. Counter to the carbon case, the low-energy feature at 5.5 eV (i) can be resolved from the bulk loss at 7 eV (ii). Two features are clearly visible at higher energies, namely, 12 eV (iii) and 17 eV (iv) and do not exhibit any noticeable shift while varying the impact parameter.

The line scan mode coupled with usual EELS facilities permits more than a simple determination of the different mode energies. The intensity profiles displayed in Fig. 3 provide a useful representation of the spatial dependence of the excitations probabilities and therefore valuable information about the nature of the excitations modes. By comparison

with the ADF profile it can be seen that bulk modes (i), (iv), and (v) (occurring for an electron beam penetrating the object) are localized in the nano-object, and no extension outside is observed.

The situation is different for modes occurring in a nonpenetrating geometry. First, the excitation probability is nonzero outside the particle and decays roughly exponentially into vacuum. Each mode shows a maximal probability on both the inner and outer surface of the tube, leading to the identification of these modes as surfaces modes. We would like to stress here the very large coupling distance between the electron beam and the particle (typically a few nanometers).

Finally, from these profiles we note that all surface modes are excited simultaneously (with different intensity probabilities) whatever the position of the electron probe into vacuum. Therefore, a simple interpretation where modes would be associated independently with inner or outer surfaces is demonstrated to be invalid here. We will come back to a further analysis of the experimental results in Sec. IV after the description of the dielectric model thereafter.

III. CLASSIC CONTINUUM DIELECTRIC MODEL FOR SURFACE PLASMON EXCITATIONS IN HIGHLY ANISOTROPIC CURVED NANOSTRUCTURES

In the present section we recall the main features of the dielectric approach for the simulation of plasmon excitations of anisotropic materials with hollow spherical or cylindrical morphology. This approach is based on the description of the ''spherical'' or ''cylindrical'' anisotropy by a dielectric tensor, locally diagonal in spherical or cylindrical coordinates.[36] The dielectric tensor of the particle is transferred from that of the planar to

$$\vec{\varepsilon}(\omega)=\varepsilon_{\parallel}(\omega)\mathbf{rr}+\varepsilon_{\perp}(\omega)(\boldsymbol{\theta\theta}+\boldsymbol{\varphi\varphi}) \tag{1}$$

in the spherical case, and to

$$\vec{\varepsilon}(\omega)=\varepsilon_{\parallel}(\omega)\mathbf{rr}+\varepsilon_{\perp}(\omega)(\mathbf{zz}+\boldsymbol{\varphi\varphi}) \tag{2}$$

in the cylindrical case.

$\varepsilon_{\perp}(\omega)$ and $\varepsilon_{\parallel}(\omega)$ are, respectively, the in-plane and out-of-plane dielectric functions (respectively, perpendicular and parallel to the anisotropy axis) of the planar material and $(\mathbf{rr},\boldsymbol{\theta\theta},\boldsymbol{\varphi\varphi})$ and $(\mathbf{rr},\mathbf{zz},\boldsymbol{\varphi\varphi})$ are, respectively, the local basis in spherical and cylindrical coordinates.

For a hollow anisotropic spherical particle, the knowledge of $\vec{\varepsilon}(\omega)$ leads to an analytic expression for the dynamic multipolar polarizability $\alpha_1(\omega)$ by resolving the nonretarded Maxwell equations and matching the boundary conditions. $\alpha_1(\omega)$ is defined as the response function of the molecule at a multipolar field of order 1 (see Refs. 35 and 36). The same procedure can be applied to an infinitely long hollow anisotropic cylindrical shell and a multipolar dynamical polarizability per unit length $\alpha_m(\omega)$ can be defined[40] (m is the azimuthal quantum number in cylindrical coordinates). $\alpha_m(\omega)$ is obtained analytically if scattering events without momentum transfer along the tube axis ($k_x=0$) are considered. However, the solution for finite momentum transfer ($k_x\neq 0$) was carried out for an isotropic cylinder without internal cavity ($r=0$).[43,44]

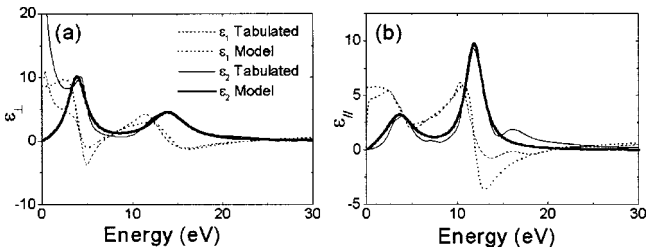

FIG. 5. Real and imaginary parts of the in-plane and out-of-plane components of the dielectric constant tabulated (Ref. 47) and in their simplified behavior within a Lorentzian model.

The EEL spectrum can then be computed for a given impact parameter outside the particle within the semiclassical approximation. As a matter of fact, the Coulomb field of an electron moving near the surface of a medium polarizes this medium. This induced electromagnetic field acts back on the electron, which suffers an energy loss. The induced electromagnetic (em) field is related to the known quantity $\alpha_1(\omega)$. Thus, assuming that the STEM electron probe is made up of classical electrons moving in a straight line, it is possible to compute the work of an electron along its trajectory as

$$W(b)=-q\int_{-\infty}^{+\infty}dt\,\mathbf{v}\cdot E^{\mathrm{ind}}[\mathbf{r}_e(t)]=\int_0^{\infty}\hbar\omega P(\omega)d(\hbar\omega), \tag{3}$$

where W is the energy loss, b the impact parameter [see Fig. 1(a)], $\mathbf{E}^{\mathrm{ind}}$ the induced field, $\mathbf{r}_e$ the position of the electron, and $\mathbf{v}$ is the classical velocity of the electron.

The EEL spectrum follows from the Fourier transform of the work with respect to time, which leads in the spherical case to[45]

$$P(b,\omega)=\sum_{l=1}^{l_{\max}}C_l(b,\omega)\mathrm{Im}[\alpha_l(\omega)], \tag{4}$$

$$C_l(b,\omega)=\frac{q^2}{4\pi\varepsilon_0\hbar^2\nu^2}(\omega/\nu)^{2l}\sum_{m=0}^{l}\frac{2-\delta_{m,0}}{(l-m)!(l+m)!}\times K_m^2(\omega b/\nu),$$

where K_m is the modified Bessel function of the second kind of order m.

In cylindrical geometry, the description of the em interaction between the electron probe and the particle is analytically more complex. And as far as we know, semianalytical solutions have only been proposed for isotropic cylinders.[46]

One of the main inputs to our model is the dielectric tensor component [Eqs. (1) and (2)]. We took this information from tabulated values for planar graphite[47] and hexagonal BN.[48] In order to be able to separate easily the contribution from each component, we have also considered a Lorentzian model for the dielectric function (see Fig. 5). We consider that the dielectric data are locally valid at any point in the material even if there is a local curvature. Such curvature effects on the local electronic polarizability have been shown to be noticeable only for small radii (less than 0.5 nm).[49]

IV. DISCUSSION

A. Bulk modes

First of all, we discuss briefly the nature of the energy features occurring when the beam intersects the nano-objects.

In the case of carbon similar to the nanoparticles, the three main modes mentioned in Sec. II are well-known bulk excitations in planar graphite. The 6–7-eV peak is commonly described as arising from the excitations of valence electrons of the π character. The $\pi+\sigma$ mode requires more extensive discussion. From the second derivative mode (inset Fig. 2) it is obvious that the broad resonance around 25 eV has to be decomposed into two modes at 23 (iv) and 27 eV (v). The shift observed for this broad mode in the normal mode as the probe is scanned from the external part of the particle to the center of the particle is then interpreted as resulting from the variation of the contribution of the two modes at 23 and 27 eV. Indeed, when compared with the ADF profile, which is correlated to the thickness profile of a hollow cylinder, the 23-eV mode intensity is found to be dominant at the edge of the object (where on average, the curved layers are oriented parallel to the beam) and relatively less intense at the center of the object (where the curved planes of the coaxial cylinder—or concentric spheres—are on average oriented perpendicular to the beam). The 27-eV mode intensity profile follows the opposite law, namely, it is dominant when the electron trajectory goes through the center of the object and becomes less intense at the edge. It is clear that the variation in the respective weights is due to an anisotropic effect. The 23-eV mode is associated to the $\varepsilon_{\parallel}(\omega)$ component and the 27-eV mode to the $\varepsilon_{\perp}(\omega)$ component of the dielectric tensor. This anisotropy of the bulk excitations has already been reported for graphite[50] and extensively studied within the framework of a dielectric model for a beam penetrating a graphitic spherical particle.[27] Moreover, similar anisotropic effects on the intensity variation of the carbon *K*-edge fine structures have been reported when moving a probe along a line scan perpendicular to a multishell carbon nanotube.[49] Finally we believe that this anisotropy effect is responsible for the discrepancies reported in the literature[24,25] concerning the energy position of the bulk $\pi+\sigma$ plasmon with respect to the size of the nanotubes. As a matter of fact, the recorded spectrum arises from a convolution of the nano-objects's response with the finite size of the probe, both quantities being of the same order of magnitude. Consequently, a change of the particle size modifies the relative weight of the contributions from the side and from the core area of the particle in the total spectrum.

With BN tubes, the same analysis can be applied. Indeed, hexagonal BN is isoelectronic to graphite[51] and collective excitations can also be described by π and $\pi+\sigma$ plasmons. They occur at 7 eV (ii), 23 eV (v), and 30 eV (vi) in the present EELS spectra (Fig. 4). So far, we do not have any comprehensive interpretation for the energy feature at 38 eV. Again the same anisotropic effect involving the 23- and 30-eV modes is observed. We also interpret this effect (combined with the surface plasmon contribution) to be responsible for the shift in the $\pi+\sigma$ bulk mode from 21.7 to 22.4 eV observed in Ref. 28 when comparing EELS spectra for a 8-nm-diameter and a 28-nm-diameter BN nanotube.

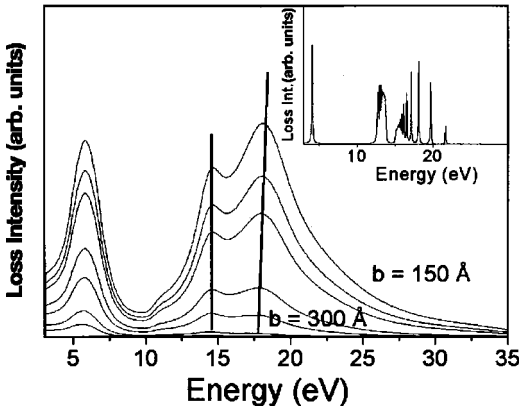

FIG. 6. Simulated EEL spectra of a 150-Å radius carbon onion for different impact parameters *b* computed with tabulated dielectric function. Impact parameter is ranging from 150 Å (surface) to 300 Å. Inset: Calculated EELS spectrum with vanishing small damping.

B. Surface modes

The following part of the discussion is devoted to the interpretation of the surface energy losses that occur when the electrons do not cross the nanoparticles. The similarities of the EELS results from the different structures studied (cylindrical or spherical, BN or C constituted) have already been stressed and we analyze here the nature of the observed modes relying on the classical continuum dielectric model as summarized previously.

1. Onions

Let us start with the case of carbon onions for which the calculation has been completely analytically driven. In Fig. 2, we clearly observe three surface modes [(i), (ii), (iii)].

Figure 6 shows, the simulation using the dielectric model, of the EELS spectra of onionlike particles ($r=1.8$ Å, $R=150$ Å, $E_0=100$ keV) for various impact parameters when the beam is not intersecting the onion. A tabulated dielectric tensor was used. Following our previous analysis,[35,40] we interpret these spectra as follows: for each family of allowed interband transitions there exists a plasmon mode for the bulk as well as for the surface. Consequently, the 6-eV (i) peak is attributed to a surface collective excitation of π electrons associated with π-π^* transitions for the in-plane dielectric function of graphite; the 17–18-eV (iii) resonance is attributed to the surface excitation of σ electrons associated with σ-σ^* transition. The weak peak at 14 eV (ii) is attributed to both π-σ^* and σ-π^* transitions.[52,53] The inset in Fig. 6 shows the EELS simulation when a Lorentzian model with a vanishingly small damping (0.1 eV) is used. This curve clarifies the origin of the major resonances observed in the simulation based on tabulated dielectric data, as resulting from the convolution by a lifetime broadening.[54,56] This behavior is somewhat different from the isotropic hollow spherical shell case where two surface modes (called tangential and radial resonances) are clearly separated.[30] Note also that the excitation scheme of a spherical shell can be related to the more studied problem of a self-supported dielectric film response. For example, an isotropic dielectric film presents two surface modes related to symmetric and antisymmetric eigenvectors that can be directly related to the tangen-

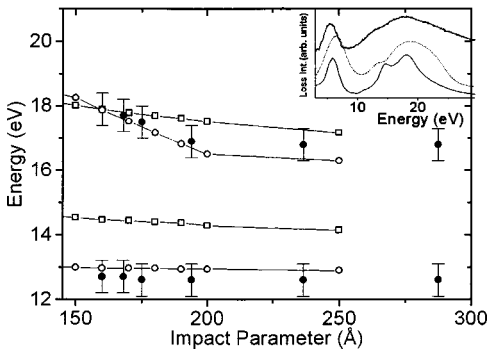

FIG. 7. Experimental (open dots and squares) and calculated (filled dots) energy positions of the different surface modes versus impact parameter for a 150 Å radius carbon onion.

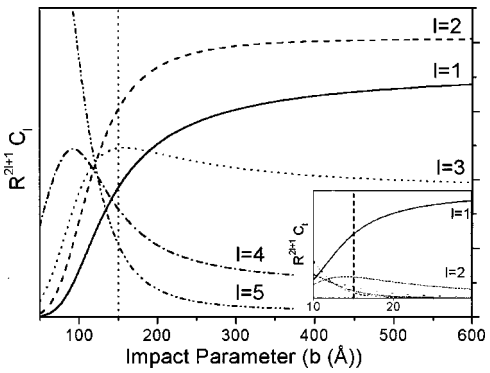

FIG. 8. Relative weights of the first multipolar terms contributing to the 15-eV mode for a carbon onion with a 150-Å external radius. The same simulation is shown in inset for a carbon onion with a 15-Å external radius.

tial and radial modes of a spherical dielectric shell.[55] For anisotropic materials, the multipeak spectra observed with spherical shells (inset Fig. 6) are similar to the complex mode structures found for an anisotropic dielectric film.[34] A further discussion on this point will be proposed in a forthcoming paper.[56]

We now further discuss how far the agreement between experiment and calculation can be good. In the inset of Fig. 7, we show an experimental EELS spectrum obtained for $R=150$ Å, $b=168$ Å, and $E=100$ keV (upper curve), and the corresponding spectra simulated with tabulated dielectric data (lower curve) and with a Lorentzian model for $\varepsilon(\omega)$ (intermediate curve).

The intense σ plasmon around 17 eV is very well reproduced by the simulations. The 15-eV mode appears as a shoulder on the increasing slope of the 17-eV σ plasmon but it is found without ambiguity in all spectra. The discrepancies in intensity and position observed for this out-of-plane mode when using dielectric data coming from different sources are related to the discrepancies found in the literature for what concerns the out-of-plane component of graphite. However, we would like to emphasize that this out-of-plane mode is always observed experimentally.

A striking behavior of the STEM-EELS spectra of carbon onions is their dependence upon the impact parameter. First, we observe an exponential decay of the surface plasmon intensity. Second, from Fig. 2 (experimental) and Fig. 6 (simulation), we can emphasize the down shift in energy of the in-plane (iii) surface mode and the constancy of the out-of-plane (ii) surface mode position when b increase. In order to highlight this phenomenon, a comparison of the peak positions of experimental and theoretical EELS spectra on carbon onionlike particles is shown in Fig. 7. We note that not only is a quantitative agreement found for the position of the peaks consecutive to the excitation of surface plasmons (except for the out-of-plane excitation described by the tabulated dielectric tensor as mentioned above) but also the shift of the in-plane mode excitation is well reproduced, as is the constancy of the out-of-plane mode with respect to impact parameter.

At this point, to account quantitatively for the near-field spectroscopy of the nanostructures, a more refined analysis of these EELS spectra features based on the dielectric theory can be developed. Coming back to Eq. (4), we see that the total loss is the sum over multipolar polarizabilities (α_1) and the weight of each term is given by the coefficient C_1. On Fig. 8, we plotted $R^{21+1}\,C_1$ (since α_1 scales with R^{21+1}, see Ref. 40) as a function of b. As expected, far from the surface, the induced field acting back on the electron is mainly a dipolar field, and with decreasing b the multipolar component with larger 1 becomes more important.[21] Furthermore, it is not only the relative intensities but also the peak positions (ω_1) in Im(α_1), which depends on 1: ω_1 increases with 1 for the in-plane resonance while it is nearly constant for the out-of-plane plasmon.[40] This change in the multipolar decomposition of the electron field thus explains the shift for the in-plane mode as a consequence of an increase in the contribution of high momentum modes with decreasing impact parameter.

The asymptotic behavior of the Bessel function is responsible for the intensity decrease at large b. As $b \gg v/\omega$ (100 Å for $\hbar\omega=10$ eV) the C_1 dependence on b, is restricted to $\exp(-\omega b/v)$ for all 1 and then, the loss peak intensity decrease is governed by an exponential function, as is well known for most of the surface losses.[20]

A similar shift to that reported here has been evidenced by other authors investigating the properties of the Si/SiO_2 planar interface.[57] A relativistic description of the electron-solid interaction was necessary to account for this behavior; which has been explained in terms of varying contributions weights of different modes with impact parameter, corresponding to different momentum transfers. We propose a similar interpretation here for spherical particles. Due to the finite size of the particles, a variation in the relative contribution of terms related to various kinetic momentum transfers is already described without including any relativistic effect. Furthermore, a relativistic counterpart of the dielectric model has been developed recently for an isotropic dielectric sphere. It was proved that for $ka<1$, where k is the excitation wave vector, a the typical size of the particle, and $v/c<1$, the relativistic effects are negligible.[58] In the present study of the $\sigma+\pi$ surface plasmon excitation in a 150-Å radius onion, $ka\approx 0.2$ and $v/c\approx 0.5$. As to the impact parameter dependence, the full relativistic calculation also leads to a Bessel function dependence and to the fact that the relative weights of the first multipolar terms do not vary sensibly for $v/c<0.5$. Thus, the present non-retarded discussion fully holds for our experimental conditions.

2. Nanotubes

We now turn to the discussion on STEM-EELS on carbon nanotubes. We have shown in Sec. II that experimental spectra from nanotubes are very similar to those on onions. This similarity is related to the similarity of the modes that occur in both nanotubes and onions when the electric field is perpendicular to the tube axis. Indeed, in-plane and out-of-plane modes involve very similar restoring forces and can be decomposed into $m=1,2,3,...$, modes for nanotubes as it was into $l=1,2,3,...$ for onions (m is here the azimuthal quantum number). We can then attribute the 6-eV (i) and 17–18-eV (iv) modes to the π-π^* and σ-σ^* in-plane surface plasmon excitations and the 14-eV (iii) mode to the π-σ^* and the σ-π^* out-of-plane excitations. Moreover, the shift of the σ-σ^* in-plane mode with impact parameter as observed experimentally for tubes can also be attributed to a variation of the relative contribution of the modes associated with different azimuthal quantum numbers m.

However, it is worth noting that a full interpretation of the EELS spectra from infinite long anisotropic cylinders is much more complex than that from spherical particles. The main reason is that cylindrical nanostructures can be described as nanoparticles in the direction perpendicular to the tube axis but they are (nearly) infinite periodic materials along the tube axis. A first consequence is that the momentum transferred by the incoming electrons to the nanotube is quantified (by the integer m) across the tube axis and is continuous along the tube axis. From the geometry of the spectrometer (see Sec. II), we can deduce that the maximum momentum transfer is of the order of 2 $Å^{-1}$. Such a large momentum transfer certainly leads to a dispersion of plasmons. In fact, a dispersion of a few eV has been measured for by EELS the volume plasmon in bundles of SWCNT.[26] The dispersion relations for MWCNT have been simulated for a curved multilayer electron gas by Yannouleas and co-workers[32,38] and in SWCNT (see, i.e., Ref. 59 and references therein). Both computations have led to a dispersion of several eV of the plasmon excitations for a momentum transfer up to 2 $Å^{-1}$. This dispersion along the tube axis has then to be included in a full description of STEM-EELS spectra for cylindrical structures, even if cinematic effects favor the excitations with a low momentum transfer. Another implication of the dispersion along the tube axis, which should be a feature of a more complete description, lies in the likely relativistic effects similar to those discussed for the planar interfaces by Moreau *et al.*[57]

The above interpretation accounts for the observed spectra of large size carbon nanotubes (more than 15 layers). For smaller nanotubes (four layers), we have not observed any systematic shift of the in-plane mode energy with the impact parameter, and the intensity of modes $I(b)$ does not show a clear exponential decrease. Indeed, for such tubes ($R=15$ Å), the dipolar contribution very rapidly becomes dominant when b decreases as demonstrated in the inset of Fig. 8. One can see that the far-field (dipolar) contribution to the total loss is already dominant for $b=20$ Å. The width of the electron beam (5 Å) is far from being negligible in the present case. As a result, the average on the width and profile of the beam blurs the expected tendency, and consequently it is then not possible to obtain any experimental evidence of such shifts.

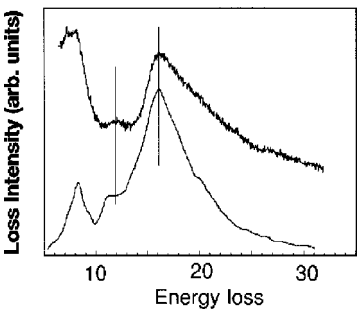

FIG. 9. Simulated EEL spectrum for a BN onion (lower curve) compared with experimental data from a BN nanotube (upper curve). The outer diameter for both objects is 4 nm.

The interpretation of BN data is based on the description of BN onion surface modes. As already quoted for bulk plasmons, collective excitations in BN nanotubes are very similar to those of carbon nanostructures as far as classification of the modes is concerned. Figure 9 shows a comparison between a simulated EEL spectrum from a BN onion and experimental data from a BN multishell nanotube. We propose an interpretation following the scheme already introduced for carbon nano-objects: the π surface plasmon (associated with π-π^* transition) and the in-plane $\pi+\sigma$ surface plasmon (associated with σ-σ^* transition) can be distinguished at 5.5 and 17 eV, respectively, and an out-of-plane plasmon associated with a σ-π^* and π-σ^* transition is also observed at 12 eV.

V. CONCLUSION

We have performed an extensive EELS-STEM study of the plasmon excitations in spherical and cylindrical layered particles (carbon onions and carbon and BN nanotubes). More specifically, we have stressed the prime importance of the anisotropy of the material in the analysis of both volume and surface excitations. Similarities in the interpretation of spherical and cylindrical compounds have been stressed, although the interpretation for nanotubes is more complex due to their one-dimensional character.

A shift of the volume plasmon from 23 to 27 eV is observed when the focussed electron beam is scanned from the edge to the center of the particle. This ''shift'' has been interpreted as a geometrical effect originating from the continuous change of the relative orientation of the layers with respect to the electrons during the scan, and consequently as a variation of the relative contribution of two volume plasmon modes usually referred to two orientations of the layers (parallel and perpendicular to the beam).

When the beam does not intersect the particles, evidence for surface plasmons was found. Combining simulations based on a dielectric theory (which fully takes the anisotropy into account), we have emphasized the prime influence of the anisotropic character of the nanoparticles on the spectra. High-energy losses (17–18 eV for carbon particles and 17 eV for BN nanotubes) were related to the σ-σ^* type of excitations associated with in-plane excitations in planar compounds. As for the surface resonances at 13 eV (carbon) and 12 eV (BN), they have been attributed to σ-π^* and

π-σ* excitations referred to as out-of-plane excitations in planar compounds. A further description of the normal modes associated with plasmon excitation in anisotropic nanostructures will be presented shortly.[56]

Another striking feature of our results is the shift of the σ surface plasmon when the impact parameter increases. The semiclassical dielectric theory leads us to attribute this phenomenon to changes in the weight of the different multipole contributions as the impact parameter changes.

The present study has been devoted to objects made of a rather important number of layers (MWCNT or onions) and the results could therefore be explained within a classical model involving a tensor of dielectric constants. The changes in the structures of smaller sizes (i.e., SWNT and bundles of those) will be discussed in a forthcoming paper.[60]

ACKNOWLEDGMENTS

We acknowledge T. Cabioc'h, N. Demoncy, H. Pascard, A. Loiseau, and P. Bernier for providing us with the samples. We also thank Ph. Lambin and A. A. Lucas for stimulating discussions and C. Searle for a careful reading of the manuscript. This work was partly funded by the Belgium National Program PAI-IUAP P4/10. L.H. was supported by the Belgium FNRS. K.S. and C.C. thank a NEDO program and a JST/CNRS ICORP collaboration for their support.

*Author to whom correspondence should be addressed.

[1] H. W. Kroto, J. R. Heath, S. C. O'Brien, R. F. Curl, and R. E. Smalley, Nature (London) **318**, 162 (1985).
[2] D. Ugarte, Nature (London) **359**, 707 (1992).
[3] S. Ijima, Nature (London) **354**, 52 (1991).
[4] O. Stéphan, Y. Bando, A. Loiseau, F. Willaime, N. Schramchenko, T. Tamiya, and T. Sato, Appl. Phys. A: Mater. Sci. Process. **67**, 107 (1998).
[5] A. Loiseau, F. Willaime, N. Demoncy, G. Hug, and H. Pascard, Phys. Rev. Lett. **76**, 4737 (1996).
[6] O. Stéphan, P. M. Ajayan, C. Colliex, Ph. Redlich, J. M. Lambert, P. Bernier, and P. Lefin, Science **266**, 966 (1995).
[7] K. Suenaga, C. Colliex, N. Demoncy, A. Loiseau, H. Pascard, and F. Willaime, Science **278**, 653 (1997).
[8] N. G. Chopra, R. J. Luyken, K. Cherrey, V. H. Crespi, M. L. Cohen, S. G. Louie, and A. Zettl, Science **269**, 966 (1995).
[9] N. Hamada, S. Sawada, and A. Oshiyama, Phys. Rev. Lett. **82**, 1579 (1992).
[10] X. Blase, A. Rubio, S. G. Louie, and M. L. Cohen, Europhys. Lett. **28**, 335 (1994).
[11] S. J. Tans, M. H. Devoret, H. Dai, A. Thess, R. E. Smalley, L. J. Georliga, and C. Dekker, Nature (London) **386**, 474 (1997).
[12] A. Kasumov, R. Deblock, M. Kociak, B. Reulet, H. Bouchiat, I. I. Khodos, Yu. B. Gorbatov, V. T. Volkov, C. Journet, and M. Burghard, Science **284**, 1508 (1999).
[13] F. Banhart, edited by P. Delhaes, in *The World of Carbon* (IOP, Bristol, 1999), Vol. 2.
[14] M. S. Dresselhaus, G. Dresselhaus, and P. C. Eklund, *Science of Fullerenes and Carbon Nanotubes* (Academic, San Diego, 1996).
[15] M. Terrones, W. K. Hsu, H. W. Kroto, and D. R. M. Walton, Top. Curr. Chem. **199**, 190 (1999).
[16] T. W. Ebbesen, H. J. Lezec, H. F. Ghoem, T. Thie, and P. A. Wolf, Nature (London) **391**, 667 (1998).
[17] U. Schroter and D. Heimann, Phys. Rev. B **58**, 15 419 (1998).
[18] D. Landbein, in *Theory of van der Waals Attraction*, Springer Tracts in Modern Physics Vol. 72 (Springer, Verlag, Berlin, 1974).
[19] S. Nie and S. R. Emory, Science **275**, 1102 (1997).
[20] R. J. Warmack, R. S. Becker, V. E. Anderson, R. H. Ritchie, Y. T. Chu, J. Little, and T. L. Ferell, Phys. Rev. B **29**, 4375 (1984).
[21] M. Achèche, C. Colliex, H. Kohl, A. Nourtier, and P. Trebbia, Ultramicroscopy **20**, 99 (1986).
[22] D. Ugarte, C. Colliex, and P. Trebbia, Phys. Rev. B **45**, 4332 (1992).
[23] P. E. Batson, Phys. Rev. Lett. **49**, 936 (1982).
[24] P. M. Ajayan, S. Iijima, and T. Ichihashi, Phys. Rev. B **47**, 6859 (1993).
[25] L. A. Bursill, P. A. Stadelmann, J. L. Peng, and S. Prawer, Phys. Rev. B **49**, 2882 (1994).
[26] T. Pichler, M. Knupfer, M. S. Golden, J. Fink, A. Rinzler, and R. E. Smalley, Phys. Rev. Lett. **80**, 4729 (1998).
[27] T. Stöckli, J. M. Bonard, A. Châtelain, Z. L. Wang, and P. Stadelmann, Phys. Rev. B **59**, 15 599 (1998); T. Stöckli, Ph.D. thesis, EPFL, Lausanne, 1999.
[28] M. Terauchi, M. Tanaka, T. Matsumoto, and Y. Saito, J. Electron Microsc. **47**, 319 (1998).
[29] L. Henrard, F. Malengreau, P. Rudolf, K. Hevesi, R. Caudano, Ph. Lambin, and Th. Cabioc'h, Phys. Rev. B **59**, 5832 (1999).
[30] G. Mie, Ann. Phys. (Leipzig) **25**, 377 (1908).
[31] C. F. Bohren and D. R. Huffman, *Absorption and Scattering of Light by Small Particles* (Wiley, New York, 1983).
[32] C. Yannouleas, E. Vigezzi, and R. A. Broglia, Phys. Rev. B **47**, 9849 (1993).
[33] T. V. Shahbazyan, I. E. Perakis, and J. Y. Bigot, Phys. Rev. Lett. **81**, 3120 (1998).
[34] Ph. Lambin, P. Senet, A. Castiaux, and L. Philippe, J. Phys. I **3**, 1417 (1993).
[35] L. Henrard, A. A. Lucas, and Ph. Lambin, Astrophys. J. **406**, 92 (1993); L. Henrard, Ph. Lambin, and A. A. Lucas, *ibid.* **487**, 719 (1997).
[36] A. A. Lucas, L. Henrard, and Ph. Lambin, Phys. Rev. B **49**, 2888 (1994).
[37] P. Apell, D. Ostling, and G. Mukhopadhyay, Solid State Commun. **87**, 219 (1993).
[38] C. Yannouleas, E. N. Bogachek, and U. Landzman, Phys. Rev. B **50**, 7977 (1994); **53**, 10 225 (1996).
[39] E. L. Wright, Nature (London) **336**, 227 (1988).
[40] L. Henrard and Ph. Lambin, J. Phys. B **29**, 5127 (1996).
[41] C. Colliex, M. Tencé, E. Lefèvre, C. Mory, H. Gu, D. Bouchet, and C. Jeanguillaume, Mikrochim. Acta **114/115**, 71 (1994).
[42] T. Cabioc'h, J. C. Girard, M. Jaouen, M. F. Denanot, and G. Hug, Europhys. Lett. **38**, 471 (1997).
[43] N. Zabala, A. Rivacoba, and P. M. Echenique, Surf. Sci. **209**, 465 (1989).
[44] A. Rivacoba, P. Apell, and N. Zabala, Nucl. Instrum. Methods Phys. Res. B **96**, 465 (1995).
[45] P. M. Echenique, A. Howie, and D. J. Weathley, Philos. Mag. B **56**, 335 (1987).
[46] G. B. Bertsh, H. Esbensen, and V. B. W. Read, Phys. Rev. B **58**, 14 031 (1998).
[47] B. T. Draine, Astrophys. J. **333**, 648 (1988); B. T. Draine, Prin-

ceton Observatory Report, Princeton, 1987 (unpublished).
[48] J. Cazaux, C. R. Seances Acad. Sci., Ser. B **270**, 70 (1969).
[49] O. Stéphan, P. M. Ajayan, C. Colliex, F. Cyrot-Lackmann, and E. Sandre, Phys. Rev. B **53**, 13 824 (1996).
[50] J. Daniels, C. V. Festenberg, H. Raether, and K. Zeppenfeld, *Optical Constants of Solids by Electron Spectroscopy*, Springer Tracts in Modern Physics Vol. 54 (Springer, Berlin, 1970), pp. 126–130.
[51] D. M. Hoffman, G. L. Doll, and P. C. Eklund, Phys. Rev. B **30**, 6051 (1984).
[52] R. Ahuja, S. Auluck, J. M. Wills, M. Aloini, B. Johansson, and O. Eriksson, Phys. Rev. B **55**, 4999 (1997).
[53] E. Tossati and F. Bassani, Nuovo Cimento Soc. Ital. Fis., B **65**, 161 (1970).
[54] L. Henrard. Ph.D. thesis, University of Namur, 1996.
[55] L. Henrard, O. Stéphan, and C. Colliex, Synth. Met. **103**, 2502 (1999).
[56] L. Henrard, N. Kociak, O. Stephan, K. Suenaga, C. Colliex, and P. Lambin (unpublished).
[57] P. Moreau, N. Brun, C. A. Walsh, C. Colliex, and A. Howie, Phys. Rev. B **56**, 6774 (1997).
[58] F. J. Garcia de Abajo, Phys. Rev. B **59**, 3095 (1999).
[59] M. F. Lin and K. W. K. Shung, Phys. Rev. B **57**, 10 183 (1998).
[60] K. Suenaga, N. Kociak, O. Stephan, L. Henrard, P. Lambin, and C. Colliex (unpublished).